Environmental Pollution 352 (2024) 124141

Contents lists available at ScienceDirect

Environmental Pollution

journal homepage: www.elsevier.com/locate/envpol

Nitrate formation mechanisms causing high concentration of $PM_{2.5}$ in a residential city with low anthropogenic emissions during cold season☆

Ji-Won Jeon [a], Sung-Won Park [a], Young-Ji Han [a,b,*], Taehyoung Lee [c], Seung-Ha Lee [d], Jung-Min Park [d], Myung-Soo Yoo [d], Hye-Jung Shin [d], Philip K. Hopke [e,f]

[a] Dept. of Environmental Science, Kangwon National University, Chuncheon, Gangwon-do, 24341, Republic of Korea
[b] Gangwon particle pollution research and management center, Kangwon National University, Chuncheon, Gangwon-do, 24341, Republic of Korea
[c] Dept. of Environmental Science, Hankuk University of Foreign Studies, Yongin, 17035, Republic of Korea
[d] Air quality research division, National Institute of Environmental Research, Incheon, 22689, Republic of Korea
[e] Institute for a Sustainable Environment, Clarkson University, Potsdam, NY, 13699, USA
[f] Dept. of Public Health Sciences, University of Rochester School of Medicine and Dentistry, Rochester, NY, 14642, USA

ARTICLE INFO

Keywords:
Particulate NO_3^-
Heterogenous reaction
Suburban
N_2O_5
Cl^- aerosol
Dust

ABSTRACT

During the cold season in South Korea, NO_3^- concentrations are known to significantly increase, often causing $PM_{2.5}$ to exceed air quality standards. This study investigated the formation mechanisms of NO_3^- in a suburban area with low anthropogenic emissions. The average $PM_{2.5}$ was 25.3 μg m^{-3}, with NO_3^- identified as the largest contributor. Ammonium-rich conditions prevailed throughout the study period, coupled with low atmospheric temperature facilitating the transfer of gaseous HNO_3 into the particulate phase. This result indicates that the formation of HNO_3 played a crucial role in determining particulate NO_3^- concentration. Nocturnal increases in NO_3^- were observed alongside increasing ozone (O_3) and relative humidity (RH), emphasizing the significance of heterogeneous reactions involving N_2O_5. NO_3^- concentrations at the study site were notably higher than in Seoul, the upwind metropolitan area, during a high concentration episode. This difference could potentially attributed to lower local NO concentrations, which enhanced the reaction between O_3 and NO_2, to produce NO_3 radicals. High concentrations of Cl^- and dust were also identified as contributors to the elevated NO_3^- concentrations.

1. Introduction

$PM_{2.5}$, with an aerodynamic diameters of 2.5 μm or less, poses significant health risk, such as exacerbation of respiratory, impaired lung function and cardiovascular disorders (Zwozdziak et al., 2016; Hamanaka and Mutlu, 2018). In 2021, in response to the increased evidence of adverse air pollution health impacts, the WHO revised the $PM_{2.5}$ annual mean air quality guideline to 5 μg m^{-3} (WHO, 2021). In South Korea, $PM_{2.5}$ concentrations have decreased since 2016 (Cha et al., 2023; Jeong et al., 2024). However, they still exceed the national ambient air quality annual standard of 15 μg m^{-3} at most of the national ambient air quality monitoring stations. Since the exceedance of annual standard for $PM_{2.5}$ is largely attributed to the high concentrations observed during winter, the identification of formation and/or emission pathways for $PM_{2.5}$ during the cold seasons is crucial to reduce the $PM_{2.5}$ health impacts. The North China Plain (NCP), which is located adjacent to the Korean peninsula has also had a decreasing trend in $PM_{2.5}$ concentrations especially in urban areas since 2016 (Lei et al., 2021). However, high concentrations of $PM_{2.5}$ still happen in cold season, even during the COVID-19 lockdown period when primary emissions significantly decreased. Severe haze events observed in NCP during winter were attributed to increased secondary formation compensating for the reduction in primary emissions (Lei et al., 2021), and recent increase of ozone (O_3) concentrations were considered as a major contributing factor to these phenomena (Sun et al., 2016; Zhang et al., 2014). O_3 has also significantly increased in South Korea not only in summer but also in winter (Yeo and Kim, 2021) probably because of the reduction in NO emissions from mobile and combustion sources (Sicard et al., 2020, 2023), suggesting a possible occurrence of $PM_{2.5}$ high concentration episodes in winter.

The concentrations of NO_3^- and its proportion to $PM_{2.5}$ are known to increase significantly, particularly during haze events in both China and

☆ This paper has been recommended for acceptance by Pavlos Kassomenos.
* Corresponding author.
E-mail address: youngji@kangwon.ac.kr (Y.-J. Han).

https://doi.org/10.1016/j.envpol.2024.124141
Received 26 February 2024; Received in revised form 29 April 2024; Accepted 9 May 2024
Available online 11 May 2024

South Korea (Kim et al., 2022b; Zhai et al., 2021). However, the emission rates of NO_x and NH_3, the precursor gases to NO_3^-, showed an overall decreasing trend in these regions. Although it is not clear that actual emissions are well reflected in the emissions inventories (Hopke and Querol, 2022), according to the National Emissions Inventory, NO_x and NH_3 emissions in South Korea decreased by about 38% and 15%, respectively, from 2017 to 2021 (National Air Emission Inventory and Research Center). Therefore, it is anticipated that there are complicated particulate NO_3^- formation mechanisms that cannot be explained by a linear relationship between precursor gases and NO_3^-. According to the previous studies, particulate NO_3^- is known to be mainly formed by 1) HNO_3 produced by photochemical oxidation of NO_2 by OH radicals during daytime [R1 to R2] (Morgan et al., 2015), 2) HNO_3 produced by a heterogenous reaction by N_2O_5 hydrolysis during nighttime [R3 to R5]. The heterogenous interaction of N_2O_5 on the surface of dust particles (Tang et al., 2012; Xia et al., 2019; Liu et al., 2020). The HNO_3 − NO_3^- partition is also involved in NO_3^- formation, which depends on temperature, relative humidity, and the availability of NH_3. The debate over the qualitative and quantitative contribution of these pathways to particulate NO_3^- is still ongoing, and the major NO_3^- formation mechanisms appear to vary in space and season.

$$NO + O_3 \rightarrow NO_2 + O_2 \quad \text{(R1)}$$

$$NO_2 + OH \rightarrow HNO_3 \quad \text{(R2)}$$

$$NO_2 + O_3 \rightarrow NO_3 + O_2 \quad \text{(R3)}$$

$$NO_3 + NO_2 \rightarrow N_2O_5 \quad \text{(R4)}$$

$$N_2O_5 + H_2O \rightarrow 2HNO_3 \quad \text{(R5)}$$

The purpose of this study is to identify the formation mechanisms of NO_3^- and the important influencing factors on enhancing NO_3^- in a suburban area with low anthropogenic emissions during the cold season. $PM_{2.5}$ and its NO_3^- concentrations were also compared with those in the upwind metropolitan region (Seoul) to illustrate the differences in NO_3^- production mechanisms between the two regions. There is still limited attention on the HNO_3 formation, which depends on the precursors, NO_x and NH_3, as well as photochemical oxidants (Fu et al., 2020). This study can provide valuable data for NO_3^- researches in small- and medium-sized residential areas, which are different from large and industrial cities with high NO_x emissions, given the severe lack of $PM_{2.5}$ studies in rural settings in Asia.

2. Method

2.1. Experiments

Form February 14 to March 14, 2022, hourly concentrations of $PM_{2.5}$ and its chemical components as well as gaseous pollutants were obtained from the Gangwon region air quality research center operated by National Institute of Environmental Research of Korea and located in a medium-sized city, Chuncheon, South Korea (Fig. S1). Because Chuncheon is in a water protection sanctuary, no large polluting industries can be established in this area. Thus, $PM_{2.5}$ emissions from anthropogenic sources are very low. The city is located approximately 100 km northeast of large metropolitan (Seoul) and major industrial areas (Incheon) (Fig. S1). Therefore, air quality can be influenced by regional range transport with prevailing westerly winds in cold season. Surrounded by mountains, the city has many artificial reservoirs, which often result in low wind speed and high relative humidity. Detailed measurement methods of $PM_{2.5}$ mass and its constituents are provided in supplementary material.

To compare NO_3^- concentration in Chuncheon with an upwind region, concentrations of $PM_{2.5}$ components and gaseous pollutants were obtained from Seoul region air quality research center where the measurement methods were identical.

Three-day backward trajectories were calculated using NOAA-HYSPLIT (Stein et al., 2015) and the meteorological data of the Global Data Assimilation System (GDAS) to describe the regional transport meteorological pattern. A detailed description of the backward trajectories and cluster analysis is provided in the supplementary material.

3. Results and discussion

3.1. Overall characteristics and importance of nitrate

The average $PM_{2.5}$ was 25.3 μg m^{-3} during the study period, and three high concentration episodes (HCEs), defined as periods in which $PM_{2.5}$ exceeded the daily national ambient air quality standard of 35 μg m^{-3} for at least 12 h, were observed. These HCEs were designated as Case 1 (Feb. 25 4 a.m. ~ Feb. 27, 4 a.m.), Case 2 (Mar. 04, 12 p.m. ~ Mar. 05, 4 a.m.), and Case 3 (Mar. 08, 7 p.m. ~ Mar. 10, 12 p.m.) (Fig. 1). The carbonaceous material includes more than carbon; therefore, organic aerosol (OA) was calculated by multiplying the OC concentration using a conversion factor of 1.8 in this study. Conversion factor for OC to OA varies depending on the composition of organic compounds, and OA emitted from biomass burning or formed secondarily has higher conversion factor because it is more oxygenated than primary aerosols emitted from fossil-fuel emissions (Chen et al., 2010; Malm et al., 2011; Hand et al., 2011). The study site is located in a medium-sized residential city with no large pollution industries, and biomass burning is the largest $PM_{2.5}$ sources in this city according to national emissions inventory. Therefore, a conversion factor of 1.8 was applied from OC to OA, a slightly higher than the typical conversion factor of 1.6 for urban sites (Turpin and Lim, 2001; Chow et al., 2015). During the sampling period, the largest contributor of $PM_{2.5}$ mass was OA (36.1%), followed by NO_3^- (29.7%), NH_4^+ (13.0%), and SO_4^{2-} (11.4%) (Table 1, Fig. 1e). The temporal change in NO_3^- was almost consistent with the temporal change in $PM_{2.5}$ and the fraction of NO_3^- to $PM_{2.5}$ attained 53% during the HCEs (Fig. 1). Alternatively, OA showed a decreased fraction during the HCE periods because NO_3^- increased (Table 1). These results indicated that HCEs of $PM_{2.5}$ occurring in cold season were mainly caused by the increased NO_3^-. Therefore, the formation mechanism of NO_3^- should be identified at this study site. NO_3^-–driven haze pollution in winter was often reported in East Asia including Korea (Kim et al., 2022a; Jeon et al., 2023) and China (Fu et al., 2020; Cheng et al., 2021).

3.2. Diurnal variation of NO_3^-

The relative contributions of photochemical and heterogenous reaction to particulate NO_3^- formation has been debated for a long time (Liu et al., 2020; Fu et al., 2020). To identify the main mechanism for NO_3^- formation, gas-particle partitioning coefficient, K_{AN}, between HNO_3 and particulate NO_3^- was first calculated (Eq. (1)). Lower temperatures correspond to higher values of K_{AN} and therefore lower equilibrium values of the NH_3 and HNO_3 gas-phase concentration.

$$HNO_3 + NH_3 \overset{K_{AN}}{\longleftrightarrow} NH_4NO_3 \quad \text{(R6)}$$

$$K_{AN} = K_{AN}(298) \bullet exp\left\{a\left(\frac{298}{T} - 1\right) + b\left[1 + ln\left(\frac{298}{T}\right) - \frac{298}{T}\right]\right\} \quad (1)$$

where, T is the ambient temperature in Kelvin, $K_{AN}(298) = 3.36 \times 10^{16}$ (atm^{-2}), $a = 75.11$, and $b = -13.5$ (Seinfeld and Pandis, 2016; Young et al., 2016). The coefficients of a and b may be influenced by various factors such as pressure, heating rate, and/or the presence of impurities in the system (Kaniewski et al., 2023). Thus, there is substantial uncertainty in their values.

During the sampling period, average atmospheric temperature was 0.2 °C, which was too low to effectively dissociate into gaseous HNO_3.

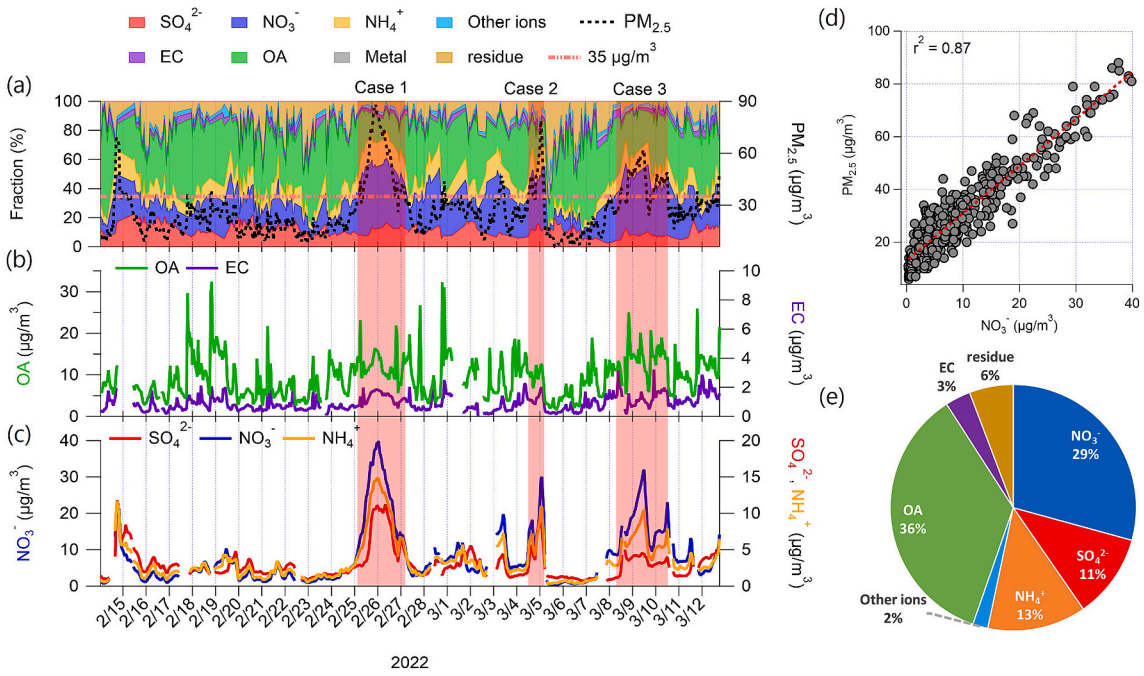

Fig. 1. (a) $PM_{2.5}$ concentrations and the fractions of its chemical components, (b) OA and EC concentrations, (c) SO_4^{2-}, NO_3^-, and NH_4^+ concentrations, (d) correlation between NO_3^- and $PM_{2.5}$, (e) pie chart of major $PM_{2.5}$ chemical components. High $PM_{2.5}$ concentration episodes (HCEs) are indicated by red block. The figures show that NO_3^- significantly increased as $PM_{2.5}$ increased. (For interpretation of the references to color in this figure legend, the reader is referred to the Web version of this article.)

Table 1
Summarized concentrations (average and standard deviation (S.D.)) of major $PM_{2.5}$ components and their fractions to $PM_{2.5}$ mass during the entire campaign and high concentration episodes designated by Case 1, Case 2, and Case 3.

	μg/m^3	NO_3^-	SO_4^{2-}	Cl^-	NH_4^+	K^+	Mg^{2+}	Ca^{2+}	OA	EC	$PM_{2.5}$
Total period	Average	7.9	3.0	0.39	3.5	0.10	0.01	0.03	9.6	0.9	27
	S.D.	7.9	2.1	0.32	2.9	0.06	0.01	0.04	4.7	0.5	15
	Fraction (%)	29.6	11.2	1.5	13.1	0.4	0.0	0.1	36.1	3.4	–
	MDL	0.017	0.003	0.011	0.030	0.023	0.002	0.010	0.24	0.00	2.4
Case 1	Average	24.2	7.0	0.83	9.5	0.16	0.01	0.03	12.2	1.4	56
	Fraction (%)	43.3	12.5	1.5	17.0	0.3	0.0	0.1	21.9	2.5	–
Case 2	Average	17.8	5.8	0.62	7.1	0.17	0.04	0.18	10.3	1.3	48
	Fraction (%)	36.9	12.0	1.3	14.7	0.4	0.1	0.4	21.1	2.7	–
Case 3	Average	18.6	3.6	0.39	6.4	0.11	0.01	0.03	14.3	1.3	46
	Fraction (%)	40.6	7.9	0.9	14.0	0.2	0.0	0.1	33.2	2.8	–

Calculated K_{AN} ranged from 1.7 x 10^{17} to 4.6 × 10^{21} atm^{-2}, which leads to the very low saturated HNO_3 concentration (average value is 0.01 ppb) when using the average NH_3 concentration of 7.7 ppb measured during the campaign. A summary of the ammonia measurements is provided in Table S1. Therefore, it can be assumed that HNO_3 is transferred to the particulate phase as it is formed.

The $[NH_4^+]/[SO_4^{2-}]$ ratio is often used as a useful quantity in calculating excess NH_4^+ (Lin et al., 2020). Theoretically, a $[NH_4^+]/[SO_4^{2-}]$ ratio value of 2.0 should demarcate the threshold between ammonium-poor and ammonium-rich regimes (Seinfeld and Pandis, 2016). In this study, approximately 96% of samples showed $[NH_4^+]/[SO_4^{2-}]$ ratio greater than 2.0 (Fig. S2), suggesting the ammonium-rich regime in general. High NO_3^- concentrations were observed with relatively high $[NH_4^+]/[SO_4^{2-}]$ ratios (Fig. S2). Therefore, NO_3^- formation was controlled by HNO_3 availability and not by NH_3 concentration in this study.

Nitrogen oxidation ratio (NOR) was calculated from the molar concentrations of NO_2 and NO_3^- (Eq. (2)). It should be noted that Eq. (3) omits a number of potentially important species such as HNO_3 and peroxyacetyl nitrate (PAN); therefore, it can provide only a qualitative measure of the degree of oxidation of NO_2.

$$NOR = \frac{[NO_3^-]}{[NO_3^-] + [NO_2]} \quad (2)$$

Several studies suggested that the secondary NO_3^- formation is active when NOR is higher than 0.1 (Fu et al., 2008; Zhang et al., 2018), and the average NOR was 0.13 in this study. Diurnal pattern of NO_3^- showed a major peak between 11:00 and 13:00, coinciding with the peak of NOR (Fig. 2). These daytime peaks of NO_3^- and NOR also appeared similar to the trends of solar radiation, suggesting that the gaseous oxidation of NO_2 by OH (R2) generally played an important role in forming HNO_3, considering that the diurnal pattern of OH concentration follows solar radiation (Ma et al., 2019). NO_2 concentration peaked about 3–4 h before NO_3^- reached its peak, probably due to the time required for oxidation to HNO_3. Considering that the rate coefficient of R2 ($k_2 = 3 \times 10^{-11}$ cm^3 molecules^{-1} s^{-1}; high pressure limit) (Seinfeld and Pandis, 2016) and the reported daytime OH concentrations in urban during winter in previous studies (2×10^6–5×10^6 molecules cm^{-3}) (Ma et al., 2019; Slater et al., 2020), the lifetime of NO_2 would be 1.9–4.6 h, which could support the time lag between NO_2 and NO_3^- observed in Fig. 2. Daytime peaks of NO_3^- and NOR observed in this study suggest the importance of gas-phase oxidation of NO_2. The concentration of

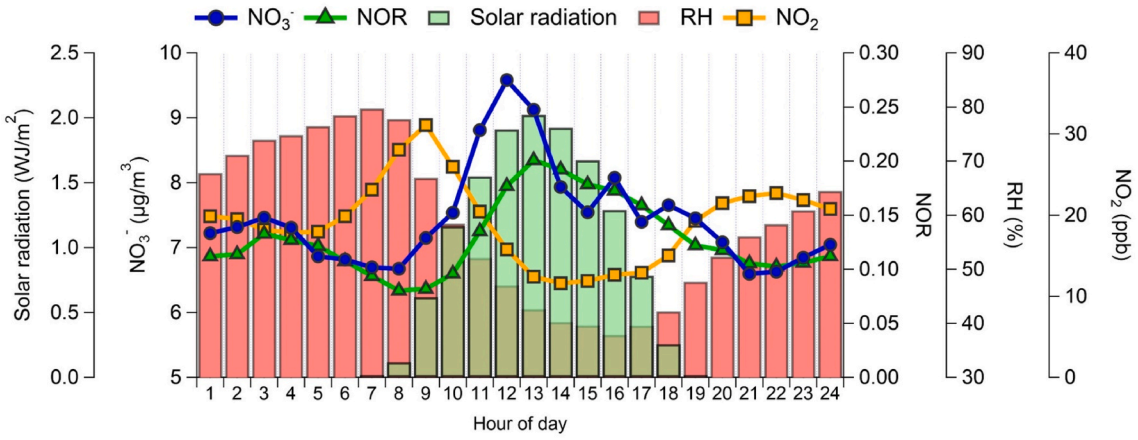

Fig. 2. Diurnal variation of NO_3^- and NO_2 along with nitrogen oxidation ratio (NOR), RH, and solar radiation. NO_3^- peaked around noon, 3 h after NO_2 peaked at 9 a.m. Both NO_3^- and NOR also showed a small peak around 3 a.m.

photochemically generated O_3 in winter is generally lower than in summer, however, the concentration of O_3 has steadily increased in Korea during winter in recent years (Yeo and Kim, 2021), which possibly results in increased production of OH and subsequent increment in daytime NO_3^- (Kim et al., 2018b; Zheng et al., 2020).

Both NOR and NO_3^- showed a small peak around 3 a.m. (Fig. 2), suggesting the effect of nocturnal chemistry in forming HNO_3. The nocturnal increment of NO_3^- will be discussed in the subsequent section.

3.3. Increment of NO_3^- during daytime and nighttime

Since HNO_3, not NH_3, was the limiting factor in producing particulate nitrate in this study, NO_3^- formation depends on the availability of NO_x and also on the oxidants that convert NO_x to NO_3^-. If gas-phase oxidation through R1 to R2 is predominant, the production of HNO_3 is determined by the concentrations of NO_2 and OH ($d[HNO_3]/dt = k_2[NO_2][OH]$). If heterogeneous oxidation through R3 to R5 is dominant, the production rate of HNO_3 is calculated by the concentrations of O_3 and NO_2 ($d[HNO_3]/dt = 2k_3[O_3][NO_2]$) when the steady state is assumed for NO_3 radical and N_2O_5 (Kim et al., 2018[1]; Young et al., 2016). Since NO_3 radical rapidly photo-dissociates, it can only play an important role at night. The correlation between NO_2 and NO_3^- was not strong both for daytime (8 a.m.–6 p.m., *Pearson* $r^2 = 0.10$, n = 284) and for nighttime (8 p.m.–6 a.m., *Pearson* $r^2 = 0.09$, n = 322), but the rate of change of NO_3^- to NO_2 increased rapidly at low RH during daytime while it increased at high RH during nighttime (Fig. S3), suggesting that NO_3^- was produced via gas-phase reaction and aqueous-phase reaction during daytime and nighttime, respectively. Also, high NO_3^- concentrations were observed with high O_3 concentration during nighttime (Fig. S3), which indicates that O_3 and RH significantly contributed to NO_3^- formation. During daytime, NO_3^- generally appeared to increase rapidly as solar radiation increased, but the impact of solar radiation on NO_3^- during daytime was not as great as the impact of O_3 on NO_3^- during nighttime (Fig. S3), probably because solar radiation was used as a proxy of OH.

In order to identify the NO_3^- formation in more detail, k_3 were calculated as follows (Seinfeld and Pandis, 2016).

$$k_3(T) = 1.2 \times 10^{-13} \exp\left(\frac{2450}{RT}\right) \quad (3)$$

During nighttime, the *Pearson* r^2 between NO_3^- and $2k_3[O_3][NO_2]$ was 0.29 (n = 295) and it increased to 0.46 between NO_3^- and the product of $2k_3[O_3][NO_2]$ and RH. NO_3^- concentrations showed a trend similar to the product of $2k_3[O_3][NO_2]$ and RH (Fig. 3). The product of $2k_3[O_3][NO_2]$ and RH closely followed the NO_3^- when high NO_3^- pollution occurred, which supports the importance of heterogeneous

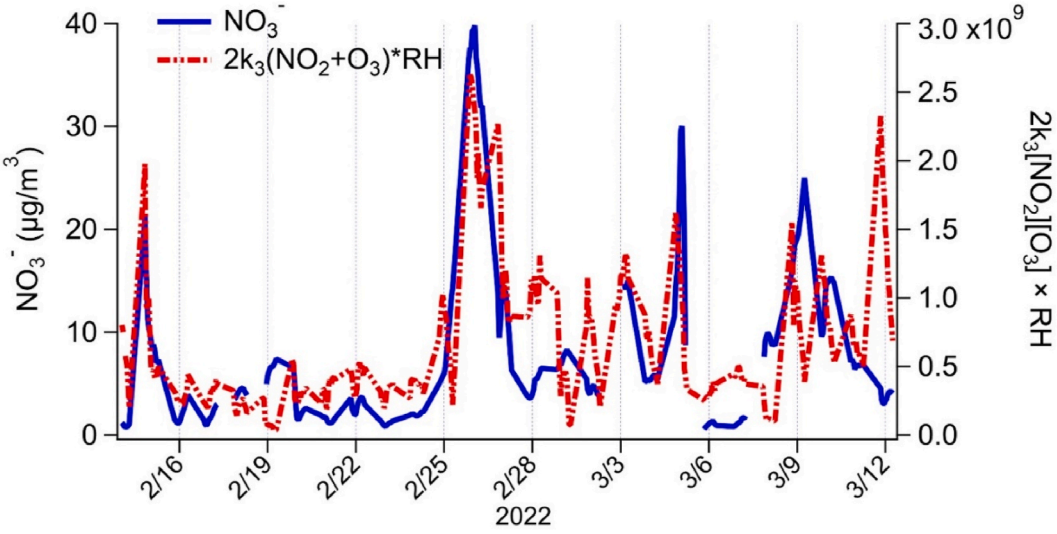

Fig. 3. Measured NO_3^- concentrations with $2k_3[NO_2][O_3]$ multiplied RH during nighttime. Two variables were followed each other very well. $2k_3[NO_2][O_3]$ was used as the estimated HNO_3 formation rate by heterogeneous reaction by N_2O_5 hydrolysis.

reactions on producing HNO_3 in this study.

Alternatively, there was no correlation between NO_3^- and the product of $k_2[NO_2]$ and solar radiation (SR) during daytime (note that k_{R2} is independent on T; Seinfeld and Pandis, 2016). However, the *Pearson* r^2 between the two variables increased to 0.13 (n = 223) when RH was less than 70%, and to 0.27 (n = 143) when RH was less than 70% and SR was greater than 1.0 MJ m^{-2}. This result suggests the general importance of gas-phase oxidation of NO_2 by OH to form HNO_3 during daytime although SR was used as a proxy of OH.

3.4. Factors influencing high concentration episodes (HCE)

In this study, three HCEs were designated as Case 1 (Feb. 25, 4 a.m. ~ Feb. 27, 4 a.m.), Case 2 (Mar. 04, 12 p.m. ~ Mar. 05, 4 a.m.), and Case 3 (Mar. 08, 7 p.m. ~ Mar. 10, 12 p.m.) (Fig. 1). For all HCEs, the concentration and fraction of NO_3^- significantly increased (Table 1). To identify the effects of regional transport, the back-trajectories were grouped into three clusters using the trajectory cluster analysis feature of HYSPLIT. Among the three clusters, clusters 1 and 3 represent the northwesterly trajectories originating from northeast China and North Korea while cluster 2 trajectories featured short trajectories confined within Korean peninsula and the adjacent ocean areas (Fig. S4). All high NO_3^- episodes were observed to be associated with cluster 2 (Fig. S4), suggesting that atmospheric stagnation after inflow, rather than long-range transport, enhanced NO_3^- concentration. Wind speeds during the HCEs were not particularly low compared to the average wind speed during the entire sampling campaign (Table S1), indicating that accumulation of $PM_{2.5}$ in near-surface level was generally not a significant factor for HCEs. During the sampling campaign, correlation was very week between wind speed and $PM_{2.5}$ (*Pearson* r^2 = 0.04, n = 640) or NO_3^- (*Pearson* r^2 = 0.01, n = 584) although their negative relationships were statistically significant. Cluster 2 were related to the highest NO_3^- fraction while clusters 1 and 3 represented higher OA fraction than cluster 2 (Fig. S4a). During the three HCEs, atmospheric temperature, RH, and the concentrations of NO_2, O_3, and NH_3 were observed to be generally high (Table S1).

In Case 1, the fraction of NO_3^- in the $PM_{2.5}$ mass was the highest (43.3%) among the three HCEs, and NO_3^- concentration showed a distinct nighttime peak (Fig. 4a). It was observed that NO_3^- was enhanced when both $2k_3[NO_2][O_3]$ and RH (60–85%) were high around at 00:00 on Feb. 26 (Fig. 4a), indicating that NO_3^- was formed by the heterogenous reaction by N_2O_5 hydrolysis followed by NO_3 radical formation. A multiple linear regression analysis showed an adjusted r^2 of 0.67 with standardized coefficients of 0.41 and 0.80 for RH and $2k_3[NO_2][O_3]$, respectively (Fig. 4c). The 3D plot shows a significant increase of NO_3^- around deliquescence relative humidity (DRH) of NH_4NO_3 (Fig. 4b) (average DRH was 75.6% during Case 1, ranging from 70.7% to 84.3%. DRH was calculated using Eq. (4) from Seinfeld and Pandis, 2016), indicating the effect of humidity on NH_4NO_3 generation and growth (Kobara et al., 2007).

$$\ln(DRH) = \frac{723.7}{T} + 1.6954 \quad (4)$$

In Case 1, Cl^- showed the highest concentrations along with highest RH among three HCEs (Table S1). Once N_2O_5 is formed through the reaction of NO_3 radical with NO_2, it can react with Cl^-, producing additional HNO_3 (R7 ~ R9). In Case 1, NO_3^- increased substantially when Cl^- increased (Fig. 4c, *Pearson* r^2 = 0.81, n = 72), once again suggesting the importance of N_2O_5 on NO_3^- formation (Xia et al., 2020; Jo et al., 2023).

$$N_2O_5(g) + Cl^-\ (het) \rightarrow Y\cdot ClNO_2(g) + (2\text{-}Y)\cdot HNO_3\ (aq) \quad (R7)$$

$$ClNO_2(g) + H_2O \rightarrow HNO_3(aq) + HCl \quad (R8)$$

$$ClNO_2(g) + OH \rightarrow HNO_3 + Cl \quad (R9)$$

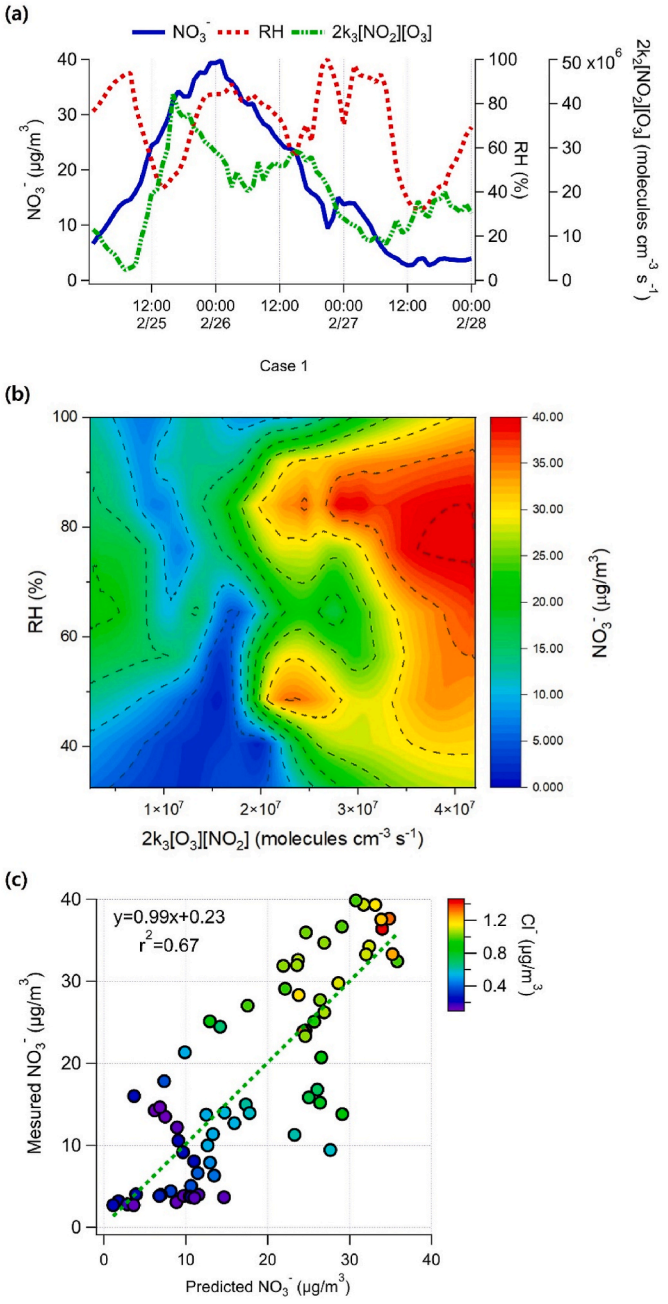

Fig. 4. (a) Temporal variation and (b) 3D plot of NO_3^-, RH, and estimated d$[HNO_3]$/dt based on R3 to R5 during Case 1, and (c) agreement between the measured NO_3^- and the predicted NO_3^- using multi-linear regression model ($NO_3^- = (-20.3 \pm 4.05) + (0.26 \pm 0.045)RH + (1.1E\text{-}6 \pm 0.00)2k_3[O_3][NO_2]$) during Case 1. In (c) panel, concentration of Cl^- was scaled by color. NO_3^- and Cl^- showed the highest concentration in Case 1 among HCEs. (For interpretation of the references to color in this figure legend, the reader is referred to the Web version of this article.)

where, Y represents the proportion of N_2O_5 reacted to form $Y\cdot ClNO_2(g)$.

In Case 2, NO_3^- concentration showed bimodal distribution with one peak during daytime and another higher peak at nighttime (Fig. 5). However, NO_3^- did not have similar trend with respect to $[NO_2][O_3]$ or RH (Fig. S5), suggesting that a different mechanism from the NO_3^- formation reactions that triggered Case 1 occurred in Case 2. The average RH during Case 2 was the lowest among three HCEs (Table S1), but it increased up to 68% during nighttime, and at the same time, Ca^{2+} and Mg^{2+} concentration significantly increased (Fig. 5). Both Ca^{2+} and Mg^{2+} showed very high concentration during Case 2 (Table 1), and relatively

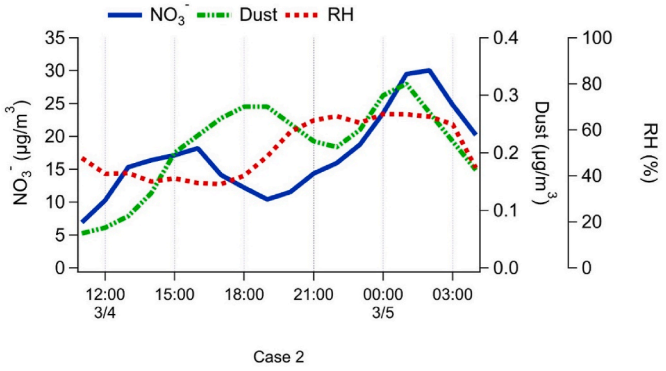

Fig. 5. Time series of NO_3^- concentration with dust and RH during Case 2. Dust concentration calculated as sum of Ca^{2+} and Mg^{2+} showed the highest value during Case 2 among HCEs.

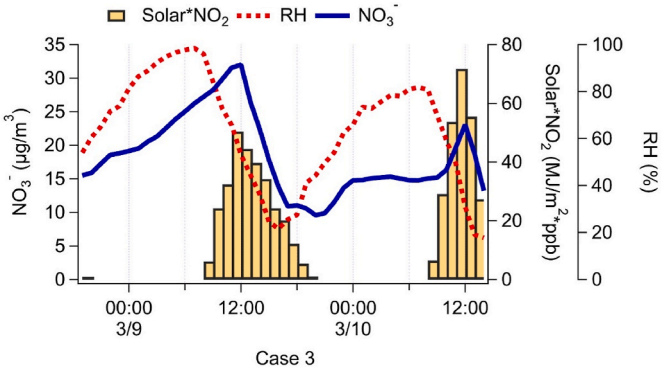

Fig. 6. Daytime peak of NO_3^- in Case 3. The variation of the product of solar radiation and NO_2 is also presented, along with RH.

high wind speeds were observed during this period (Table S1). Previous studies have suggested that dust (e.g. $CaCO_3$) not only enhances the uptake coefficient of HNO_3 to its surface under humid condition (Jia et al., 2021; Li et al., 2023) and they also adsorb the alkaline NH_3 gas (Sullivan et al., 2007). NH_3 was observed to have notably high concentration in Case 2 (Table S1). N_2O_5 can also be hydrolyzed on the surface of dust and further neutralized by NH_3 to NH_4NO_3 at nighttime. There was no correlation between NO_3^- and excess NH_4^+ ($[NH_4^+]_{eq} - [SO_4^{2-}]_{eq}$) during Case 2 (*Pearson* $r^2 = 0.07$, n = 57), indicating that NO_3^- was bound not only to NH_4^+ but also to other cations such as Ca^{2+} and Mg^{2+} (Fig. S6) while the correlation between NO_3^- and excess NH_4^+ was very strong in both Case 1(*Pearson* $r^2 = 0.996$, n = 72) and Case 3 (*Pearson* $r^2 = 0.990$, n = 112). The size distribution also showed the occurrence of coarse particles (1.0–2.5 μm) only in Case 2 (Fig. S7), supporting the formation of $Ca(NO_3)_2$ and/or $Mg(NO_3)_2$ as dust particles are mainly present in coarse mode Wu et al. (2020)]. These results suggest that very high concentrations of dust ($Ca^{2+} + Mg^{2+}$) played an important role in the formation of NO_3^- at nighttime during Case 2. During nighttime in Case 2, Cl^- concentration also increased as NO_3^- increased (*Pearson* $r^2 = 0.61$), which suggests, once again, the importance of Cl^- on nocturnal formation of HNO_3 (R7~R9). In this study, Cl^- typically showed a daytime peak (Fig. S8). In both Cases 1 and 2, Cl^- increased at nighttime along with K^+, a typical tracer for biomass burning (Hopke et al., 2020). Generally, Cl^- is considered to be emitted either from ocean as sea-salt or from coal combustion. However, biomass burning is also an important source for Cl^- (Hopke et al., 2020). The result implies that the formation of NO_3^- occurred due to the significant presence of oxidants such as OH• and ROO• in the biomass-burning plumes (Mao et al., 2013; Tuet et al., 2019; Wong et al.., 2019), which were also suggested in previous study (Choi et al., 2021). In Case 2, Ca^{2+} and Mg^{2+} during daytime (0.19 μg m^{-3}) were lower than those at night (0.25 μg m^{-3}), but still showed high concentrations. It has been suggested that mineral dust can not only directly participate in heterogeneous reactions but also affect photochemical reactions in the atmosphere as a catalyst (Li et al., 2024). Therefore, NO_2 is photocatalyzed to produce HONO on the illuminated surface of dust particle, subsequently producing OH radical via photolysis, which can induce gas-phase oxidation of NO_2.

Case 3 also showed high NO_3^- concentration contributing 40.5% of $PM_{2.5}$ mass (Table 1). NO_3^- clearly showed the daytime peak as solar radiation increased (Fig. 6), suggesting the gas-phase oxidation of NO_2 by OH. As gas-phase oxidation dominated during this period, SO_4^{2-} concentration and its fraction to $PM_{2.5}$ were the lowest in Case 3 among three HCEs (Table 1) because SO_4^{2-} is predominantly produced by heterogeneous reactions (An et al., 2019; Wang et al., 2021). In addition, the correlation between sulfur oxidation ratio (SOR = $[SO_4^{2-}]/([SO_4^{2-}]+[SO_2])$ and NOR was lowest for Case 3 (*Pearson* $r^2 = 0.12$, n = 109) compared to Case 1 (*Pearson* $r^2 = 0.55$, n = 72) and Case 2 (*Pearson* $r^2 = 0.64$, n = 57). Even in Case 1 and Case 2, where heterogeneous reactions are expected to dominate, no substantial correlation was found between SO_2 and SO_4^{2-}, suggesting that SO_4^{2-} concentrations were mainly influenced by regional- or long-range transport than local production, as suggested in previous studies conducted in Korea (Lee et al., 2023; Lee et al., 2024).

3.5. Comparison with an upwind region

When comparing $PM_{2.5}$ concentrations between Seoul (the upwind area, Fig. S1) and Chuncheon during the campaign, they exhibited very similar trends in both cities (Fig. S9a). NO_3^- concentrations in the two regions also varied similarly, but NO_3^- concentrations were approximately 10 μg m^{-3} higher in Chuncheon than in Seoul during Case 1 (Fig. S9b). This result suggests that NO_3^- was additionally produced locally in Chuncheon or during the transport of air masses from Seoul, an upwind region, to Chuncheon, a downwind region.

Since no large anthropogenic sources are located in Chuncheon, and there are not as many automobiles as in Seoul, NO concentrations were much lower in Chuncheon than in Seoul (NO concentrations were not measured in Seoul region air quality research center; therefore, a yearly averaged NO concentration in 2022 was obtained from Seoul Metropolitan Government (2022) and used in Fig. S10), while NO_2 concentrations were similar in both regions during Case 1 (Fig. S10). On the other hand, O_3 concentrations were somewhat higher in Chuncheon than in Seoul (Fig. S10). Considering that the reaction coefficient of R1 ($k_1 = 3.0 \times 10^{-13} \exp\left(\frac{1500}{RT}\right)$) is much higher than k_3, O_3 is likely to react with NO than with NO_2. However, in Chuncheon, where NO was significantly lower than NO_2, especially during nighttime (Fig. S10 and Fig. S11), the rate of O_3 reacting with NO_2 increased, subsequently effectively producing NO_3 radical (via R3). The very high RH in this city (Fig. S10) must be another crucial factor enhancing a heterogenous reaction by N_2O_5 hydrolysis to produce HNO_3 during nighttime (via R4 and R5) in Case 1.

In addition, the largest $PM_{2.5}$ source is biomass burning in Chuncheon according to the national emissions inventory (Clean Air Policy Support System). During Case 1 and Case 2 when the nighttime peaks of NO_3^- were observed, NO_3^- significantly increased when Cl^- increased, and there was a strong correlation between Cl^- and K^+ (for Case 1, *Pearson* $r^2 = 0.27$, n = 72; for Case 2, *Pearson* $r^2 = 0.71$, n = 57), implying that active biomass burning played another important role in enhancing NO_3^-. The first NO_3^- peak in Case 3 was observed only in Chuncheon (Fig. S9b). NO_2 showed the highest concentration, and the wind speed was distinctly low in Case 3, compared to those in Cases 1 and 2 (Table S1, Fig. S4), which might cause atmospheric stagnation after NO_3^- formation in Chuncheon. During Case 3, NO_2 concentration in Chuncheon (29.0 ppb) was higher than in Seoul (24.7 ppb).

4. Conclusions

In this study, the formation mechanisms of NO_3^- and the important influencing factors for enhancing NO_3^- were identified in suburban area with low anthropogenic emissions during the cold season. NO_3^- was the most substantial contributor to $PM_{2.5}$ during the campaign, and it was notably elevated particularly during high $PM_{2.5}$ concentration episodes (HCEs). The ambient temperature was low enough to almost completely transfer HNO_3(g) into the particulate phase, forming particulate NO_3^- in ammonium-rich regimes in this study. Throughout the campaign, NO_3^- and nitrogen oxidation ratio (NOR) generally exhibited daytime peaks, suggesting the general importance of gaseous oxidation of NO_2 by OH. However, two of the three HCEs observed in this study showed distinct nighttime peaks, indicating nocturnal chemistry forming HNO_3 to enhance $PM_{2.5}$ subsequent to particulate NO_3^-. During nighttime, NO_3^- significantly increased when O_3 concentration and RH increased, suggesting the important role of heterogeneous reactions involving N_2O_5. For the HCEs showing nighttime NO_3^- peaks, high concentrations of Cl^- and dust were observed, suggesting that these also contributed to NO_3^- formation. In this study, there are limitations in inferring particulate NO_3^- concentrations because important reactants and products of R1 to R5, such as HNO_3, OH, N_2O_5, and NO_3•, were not measured. It will be essential to directly measure all these species to fully understand particulate nitrate formation in future studies. Although outside transport cannot be ignored for high NO_3^- concentration, the results strongly suggest significant local production of HNO_3 in this city. In order to reduce NO_3^- and $PM_{2.5}$ concentrations in winter, comprehensive policies to reduce precursor gases and to suppress biomass burning activity should be effectively applied. An ozone reduction policy must also be considered simultaneously since HNO_3 formation depended not only on the availability of NO_x but also on O_3 concentration.

CRediT authorship contribution statement

Ji-Won Jeon: Writing – original draft, Visualization, Investigation, Formal analysis. **Sung-Won Park:** Visualization, Investigation. **Young-Ji Han:** Writing – review & editing, Validation, Supervision, Methodology, Funding acquisition, Conceptualization. **Taehyoung Lee:** Writing – review & editing, Validation, Funding acquisition. **Seung-Ha Lee:** Resources, Methodology. **Jung-Min Park:** Validation, Funding acquisition. **Myung-Soo Yoo:** Project administration. **Hye-Jung Shin:** Resources, Data curation. **Philip K. Hopke:** Writing – review & editing.

Declaration of competing interest

The authors declare that they have no known competing financial interests or personal relationships that could have appeared to influence the work reported in this paper.

Data availability

Data will be made available on request.

Acknowledgements

This research was supported by grant from the National Research Foundation of Korea [NRF-2020R1A2C2013445] and by National Institute of Environmental Research [NIER-2024-01-01-004]. This research was also supported by the FRIEND (Fine Particle Research Initiative in East Asia Considering National Differences) Project through the National Research Foundation of Korea (NRF) funded by the Ministry of Science and ICT [NRF-2023M3G1A1090663], by Particulate Matter Management Specialized Graduate Program through the Korea Environmental Industry & Technology Institute (KEITI) funded by the Ministry of Environment (MOE), and by the Core Technology Development Project for Environmental Disease Prevention and Management through the KEITI funded by the MOE [grant number 2022-KE002052].

Appendix A. Supplementary data

Supplementary data to this article can be found online at https://doi.org/10.1016/j.envpol.2024.124141.

References

An, Z., Huang, R.J., Zhang, R., Tie, X., Li, G., Cao, J., Zhou, W., Shi, Z., Han, Y., Gu, Z., Ji, Y., 2019. Severe haze in northern China: a synergy of anthropogenic emissions and atmospheric processes. Proc. Natl. Acad. Sci. U.S.A. 116 (18), 8657–8666. https://doi.org/10.1073/pnas.1900125116.

Cha, Y., Song, C.K., Jeon, K. ho, Yi, S.M., 2023. Factors affecting recent PM2.5 concentrations in China and South Korea from 2016 to 2020. Sci. Total Environ. 881 https://doi.org/10.1016/j.scitotenv.2023.163524.

Chen, L.W.A., Verburg, P., Shackelford, A., Zhu, D., Susfalk, R., Chow, J.C., Watson, J.G., 2010. Moisture effects on carbon and nitrogen emission from burning of wildland biomass. Atmos. Chem. Phys. 10 (14), 6617–6625. https://doi.org/10.5194/acp-10-6617-2010.

Cheng, C., Shi, M., Liu, W., Mao, Y., Hu, J., Tian, Q., Chen, Z., Hu, T., Xing, X., Qi, S., 2021. Characteristics and source apportionment of water-soluble inorganic ions in PM2.5 during a wintertime haze event in Huanggang, central China. Atmos. Pollut. Res. 12 (1), 111–123. https://doi.org/10.1016/j.apr.2020.08.026.

Choi, S.Y., Park, S.W., Byun, J.Y., Han, Y.J., 2021. Characteristics of locally occurring high pm2.5 concentration episodes in a small city in South Korea. Atmosphere 12 (1), 1–16. https://doi.org/10.3390/atmos12010086.

Chow, J.C., Lowenthal, D.H., Chen, L.W.A., Wang, X., Watson, J.G., 2015. Mass reconstruction methods for PM2.5: a review. Air Quality, Atmosphere and Health 8 (3), 243–263. https://doi.org/10.1007/s11869-015-0338-3.

Fu, Q., Zhuang, G., Wang, J., Xu, C., Huang, K., Li, J., Hou, B., Lu, T., Streets, D.G., 2008. Mechanism of formation of the heaviest pollution episode ever recorded in the Yangtze River Delta, China. Atmos. Environ. 42 (9), 2023–2036. https://doi.org/10.1016/j.atmosenv.2007.12.002.

Fu, X., Wang, T., Gao, J., Wang, P., Liu, Y., Wang, S., Zhao, B., Xue, L., 2020. Persistent heavy winter nitrate pollution driven by increased photochemical oxidants in northern China. Environ. Sci. Technol. 54 (7), 3881–3889. https://doi.org/10.1021/acs.est.9b07248.

Hamanaka, R.B., Mutlu, G.M., 2018. Particulate matter air pollution: effects on the cardiovascular system. In: Frontiers in Endocrinology, vol. 9. Frontiers Media S.A. https://doi.org/10.3389/fendo.2018.00680.

Hand, J.L., Copeland, S.A., McDade, C.E., Day, D.E., Moore, J.C.T., Dillner, A.M., Pitchford, M.L., Indresand, H., Schichtel, B.A., Malm, W.C., Watson, J.G., 2011. Spatial and Seasonal Patterns and Temporal Variability of Haze and its Constituents in the United States. IMPROVE Report V. Cooperative Institute for Research in the Atmosphere, Fort Collins.

Hopke, P.K., Dai, Q., Li, L., Feng, Y., 2020. Global review of recent source apportionments for airborne particulate matter. Sci. Total Environ. 740 https://doi.org/10.1016/j.scitotenv.2020.140091. Elsevier B.V.

Hopke, P.K., Querol, X., 2022. Is Improved Vehicular NOx Control Leading to Increased Urban NH3Emissions?. In: *Environmental Science and Technology*, (Vol. 56, Issue 17,. American Chemical Society, pp. 11926–11927. https://doi.org/10.1021/acs.est.2c04996.

Jeon, J., Chen, Y., Kim, H., 2023. Influences of meteorology on emission sources and physicochemical properties of particulate matter in Seoul, Korea during the heating period. Atmos. Environ. 303 https://doi.org/10.1016/j.atmosenv.2023.119733.

Jeong, J.I., Park, R.J., Song, C.K., Yeh, S.W., Woo, J.H., 2024. Quantitative analysis of winter PM2.5 reduction in South Korea, 2019/20 to 2021/22: contributions of meteorology and emissions. Sci. Total Environ. 907 https://doi.org/10.1016/j.scitotenv.2023.168179.

Jia, X., Gu, W., Peng, C., Li, R., Chen, L., Wang, H., Wang, H., Wang, X., Tang, M., 2021. Heterogeneous reaction of CaCO3 with NO2 at different relative humidities: kinetics, mechanisms, and impacts on aerosol hygroscopicity. J. Geophys. Res. Atmos. 126 (11) https://doi.org/10.1029/2021JD034826.

Jo, H.Y., Park, J., Heo, G., Lee, H.J., Jeon, W., Kim, J.M., Kim, S., Kim, J.K., Liu, Y., Liu, P., Zhang, B., Kim, C.H., 2023. Interpretation of the effects of anthropogenic chlorine on nitrate formation over northeast Asia during KORUS-AQ 2016. Sci. Total Environ. 894 https://doi.org/10.1016/j.scitotenv.2023.164920.

Kaniewski, M., Biegun, M., Hoffmann, J., 2023. Thermal stability of ammonium nitrate systems containing d-metal nitrate salts under limited mass transfer conditions. J. Therm. Anal. Calorim. 148, 5309–5323.

Kim, N.K., Kim, Y.P., Shin, H.J., Lee, J.Y., 2022b. Long-Term trend of the levels of ambient air pollutants of a megacity and a background area in Korea. Appl. Sci. 12 (8) https://doi.org/10.3390/app12084039.

Kim, H., Zhang, Q., Heo, J., 2018a. Influence of intense secondary aerosol formation and long-range transport on aerosol chemistry and properties in the Seoul Metropolitan Area during spring time: results from KORUS-AQ. Atmos. Chem. Phys. 18 (10), 7149–7168. https://doi.org/10.5194/acp-18-7149-2018.

Kim, D. young, de Foy, B., Kim, H., 2022a. The investigations on organic sources and inorganic formation processes and their implications on haze during late winter in Seoul, Korea. Environ. Res. 212 https://doi.org/10.1016/j.envres.2022.113174.

Kim, S., Jeong, D., Sanchez, D., Wang, M., Seco, R., Blake, D., Meinardi, S., Barletta, B., Hughes, S., Jung, J., Kim, D., Lee, G., Lee, M., Ahn, J., Lee, S.D., Cho, G., Sung, M.Y.,

Lee, Y.H., Park, R., 2018b. The controlling factors of photochemical ozone production in Seoul, South Korea. Aerosol Air Qual. Res. 18 (9), 2253–2261. https://doi.org/10.4209/aaqr.2017.11.0452.

Kobara, H., Takeuchi, K., Ibusuki, T., 2007. Effect of Relative Humidity on Aerosol Generation through Experiments at Low Concentrations of Gaseous Nitric Acid and Ammonia, (Vol. 7, Issue 2).. Aerosol and Air Quality Research.

Lee, G., Ahn, J., Park, S.M., Moon, J., Park, R., Sim, M.S., Choi, H., Park, J., Ahn, J.Y., 2023. Sulfur isotope-based source apportionment and control mechanisms of PM2.5 sulfate in Seoul, South Korea during winter and early spring (2017–2020). Sci. Total Environ. 905 https://doi.org/10.1016/j.scitotenv.2023.167112.

Lee, S.-J., Ju, J.-T., Lee, J.-J., Song, C.-K., Shin, S.-A., Jung, H.-J., Shin, H.J., Choi, S.-D., 2024. Mapping nationwide concentrations of sulfate and nitrate in ambient PM2.5 in South Korea using machine learning with ground observation data. Sci. Total Environ. 926, 171884 https://doi.org/10.1016/j.scitotenv.2024.171884.

Lei, L., Zhou, W., Chen, C., He, Y., Li, Z., Sun, J., Tang, X., Fu, P., Wang, Z., Sun, Y., 2021. Long-term characterization of aerosol chemistry in cold season from 2013 to 2020 in Beijing, China. Environ. Pollut. 268 https://doi.org/10.1016/j.envpol.2020.115952.

Li, J., Zhang, N., Tian, P., Zhang, M., Shi, J., Chang, Y., Zhang, L., Liu, Z., Wang, Y., 2023. Significant roles of aged dust aerosols on rapid nitrate formation under dry conditions in a semi-arid city. Environ. Pollut. 336 https://doi.org/10.1016/j.envpol.2023.122395.

Li, X., Yu, Z., Yue, M., Liu, Y., Huang, K., Chi, X., Nie, W., Ding, A., Dong, X., Wang, M., 2024. Impact of mineral dust photocatalytic heterogeneous chemistry on the formation of the sulfate and nitrate: a modelling study over East Asia. Atmos. Environ. 316 https://doi.org/10.1016/j.atmosenv.2023.120166.

Lin, Y.-C., Zhang, Y.-L., Fan, M.-Y., Bao, M., 2020. Heterogeneous formation of particulate nitrate under ammonium-rich regimes during the high-PM2.5 events in Nanjing, China. Atmospheric Chemistry and Physics 20 (6), 3999–4011. https://doi.org/10.5194/acp-20-3999-2020.

Liu, P., Ye, C., Xue, C., Zhang, C., Mu, Y., Sun, X., 2020. Formation mechanisms of atmospheric nitrate and sulfate during the winter haze pollution periods in Beijing: Gas-phase, heterogeneous and aqueous-phase chemistry. Atmos. Chem. Phys. 20 (7), 4153–4165. https://doi.org/10.5194/acp-20-4153-2020.

Ma, X., Tan, Z., Lu, K., Yang, X., Liu, Y., Li, S., Li, X., Chen, S., Novelli, A., Cho, C., Zeng, L., Wahner, A., Zhang, Y., 2019. Winter photochemistry in Beijing: Observation and model simulation of OH and HO2 radicals at an urban site. Sci. Total Environ. 685, 85–95. https://doi.org/10.1016/j.scitotenv.2019.05.329.

Malm, W.C., Schichtel, B.A., Pitchford, M.L., 2011. Uncertainties in PM2.5 Gravimetric and speciation measurements and what we can learn from them. J. Air Waste Manag. Assoc. 61 (11), 1131–1149. https://doi.org/10.1080/10473289.2011.603998.

Mao, J., Horowitz, L.W., Naik, V., Fan, S., Liu, J., Arlene, M., Fiore, 2013. Sensitivity of tropospheric oxidants to biomass burning emissions: implications for radiative forcing. Geophys. Res. Lett. 40, 1241–1246.

Morgan, W.T., Ouyang, B., Allan, J.D., Aruffo, E., di Carlo, P., Kennedy, O.J., Lowe, D., Flynn, M.J., Rosenberg, P.D., Williams, P.I., Jones, R., McFiggans, G.B., Coe, H., 2015. Influence of aerosol chemical composition on N2O5 uptake: airborne regional measurements in northwestern Europe. Atmos. Chem. Phys. 15 (2), 973–990. https://doi.org/10.5194/acp-15-973-2015.

Seinfeld, J.H., Pandis, S.N., 2016. Atmospheric Chemistry and Physics: from Air Pollution to Climate Change. John Wiley & Sons., Hoboken, New Jersey, USA.

Seoul Metropolitan Government, Air Quality Policy Division (2022) 2022 Seoul air quality report (Publication No. 51-6110000-000625-10) , Retrieved from https://news.seoul.go.kr/env/files/2023/12/65975187ece8c6.75453462.pdf.

Sicard, P., Paoletti, E., Agathokleous, E., Araminienė, V., Proietti, C., Coulibaly, F., de Marco, A., 2020. Ozone weekend effect in cities: deep insights for urban air pollution control. Environ. Res. 191 https://doi.org/10.1016/j.envres.2020.110193.

Sicard, P., Agathokleous, E., Anenberg, S.C., de Marco, A., Paoletti, E., Calatayud, V., 2023. Trends in urban air pollution over the last two decades: a global perspective. Sci. Total Environ. 858 https://doi.org/10.1016/j.scitotenv.2022.160064. Elsevier B.V.

Slater, E.J., Whalley, L.K., Woodward-Massey, R., Ye, C., Lee, J.D., Squires, F., Hopkins, J.R., Dunmore, R.E., Shaw, M., Hamilton, J.F., Lewis, A.R., Crilley, L.R., Kramer, L., Bloss, W., Vu, T., Sun, Y., Xu, W., Yue, S., Ren, L., et al., 2020. Elevated levels of OH observed in haze events during wintertime in central Beijing. Atmos. Chem. Phys. 20 (23), 14847–14871. https://doi.org/10.5194/acp-20-14847-2020.

Stein, A.F., Draxler, R.R., Rolph, G.D., Stunder, B.J., Cohen, M.D., Ngan, F., 2015. NOAA's HYSPLIT atmospheric transport and dispersion modeling system. Bull. Am. Meteorol. Soc. 96, 2059–2077.

Sullivan, R.C., Guazzotti, S.A., Sodeman, D.A., Prather, K.A., 2007. Direct observations of the atmospheric processing of Asian mineral dust. Atmos. Chem. Phys. 7. www.atmos-chem-phys.net/7/1213/2007/.

Sun, L., Xue, L., Wang, T., Gao, J., Ding, A., Cooper, O.R., Lin, M., Xu, P., Wang, Z., Wang, X., Wen, L., Zhu, Y., Chen, T., Yang, L., Wang, Y., Chen, J., Wang, W., 2016. Significant increase of summertime ozone at mount Tai in central eastern China. Atmos. Chem. Phys. 16 (16), 10637–10650. https://doi.org/10.5194/acp-16-10637-2016.

Tang, M.J., Thieser, J., Schuster, G., Crowley, J.N., 2012. Kinetics and mechanism of the heterogeneous reaction of N 2O 5 with mineral dust particles. Phys. Chem. Chem. Phys. 14 (24), 8551–8561. https://doi.org/10.1039/c2cp40805h.

Tuet, W.Y., Liu, F., de Oliveira Alves, N., Fok, S., Artaxo, P., Vasconcellos, P., Champion, J.A., Ng, N.L., 2019. Chemical oxidative potential and cellular oxidative stress from open biomass burning aerosol. Environ. Sci. Technol. Lett. 6, 126–132. https://doi.org/10.1021/acs.estlett.9b00060.

Turpin, B.J., Lim, H.J., 2001. Species contributions to $PM_{2.5}$ mass concentrations: revisiting common assumptions for estimating organic mass. Aerosol Sci. Technol. 35, 602–610.

Wang, S., Wang, L., Wang, N., Ma, S., Su, F., Zhang, R., 2021. Formation of droplet-mode secondary inorganic aerosol dominated the increased PM2.5 during both local and transport haze episodes in Zhengzhou, China. Chemosphere 269. https://doi.org/10.1016/j.chemosphere.2020.128744.

WHO, 2021. WHO global air quality guidelines: particulate matter (PM2.5 and PM10), ozone, nitrogen dioxide, sulfur dioxide and carbon monoxide. World Health Organization, Geneva. URL https://apps.who.int/iris/handle/10665/345329 (accessed 01.08.22).

Wong, J.P., Tsagkaraki, M., Tsiodra, I., Mihalopoulos, N., Violaki, K., Kanakidou, M., Sciare, J., Nenes, A., Weber, R.J., 2019. Effects of atmospheric processing on the oxidative potential of biomass burning organic aerosols. Environ. Sci. Technol. 53, 6747–6756. https://doi.org/10.1021/acs.est.9b01034.

Wu, C., Zhang, S., Wang, G., Lv, S., Li, D., Liu, L., Li, J., Liu, S., Du, W., Meng, J., Qiao, L., Zhou, M., Huang, C., Wang, H., 2020. Efficient heterogeneous formation of ammonium nitrate on the saline mineral particle surface in the atmosphere of East Asia during dust storm periods. Environ. Sci. Technol. 54 (24), 15622–15630. https://doi.org/10.1021/acs.est.0c04544.

Xia, M., Wang, W., Wang, Z., Gao, J., Li, H., Liang, Y., Yu, C., Zhang, Y., Wang, P., Zhang, Y., Bi, F., Cheng, X., Wang, T., 2019. Heterogeneous uptake of N2O5 in sand dust and urban aerosols observed during the dry season in Beijing. Atmosphere 10 (4). https://doi.org/10.3390/ATMOS10040204.

Xia, M., Peng, X., Wang, W., Yu, C., Sun, P., Li, Y., Liu, Y., Xu, Z., Wang, Z., Xu, Z., Nie, W., Ding, A., Wang, T., 2020. Significant production of $ClNO_2$ and possible source of Cl_2 from N_2O_5 uptake at a suburban site in eastern China. Atmos. Chem. Phys. 20 (10), 6147–6158. https://doi.org/10.5194/acp-20-6147-2020.

Yeo, M.J., Kim, Y.P., 2021. Long-term trends of surface ozone in Korea. J. Clean. Prod. 294 https://doi.org/10.1016/j.jclepro.2020.125352.

Young, D.E., Kim, H., Parworth, C., Zhou, S., Zhang, X., Cappa, C.D., Seco, R., Kim, S., Zhang, Q., 2016. Influences of emission sources and meteorology on aerosol chemistry in a polluted urban environment: results from DISCOVER-AQ California. Atmos. Chem. Phys. 16 (8), 5427–5451. https://doi.org/10.5194/acp-16-5427-2016.

Zhai, S., Jacob, D.J., Wang, X., Liu, Z., Wen, T., Shah, V., Li, K., Moch, J.M., Bates, K.H., Song, S., Shen, L., Zhang, Y., Luo, G., Yu, F., Sun, Y., Wang, L., Qi, M., Tao, J., Gui, K., et al., 2021. Control of particulate nitrate air pollution in China. Nat. Geosci. 14 (6), 389–395. https://doi.org/10.1038/s41561-021-00726-z.

Zhang, Q., Yuan, B., Shao, M., Wang, X., Lu, S., Lu, K., Wang, M., Chen, L., Chang, C.C., Liu, S.C., 2014. Variations of ground-level O3 and its precursors in Beijing in summertime between 2005 and 2011. Atmos. Chem. Phys. 14 (12), 6089–6101. https://doi.org/10.5194/acp-14-6089-2014.

Zhang, R., Sun, X., Shi, A., Huang, Y., Yan, J., Nie, T., Yan, X., Li, X., 2018. Secondary inorganic aerosols formation during haze episodes at an urban site in Beijing, China. Atmos. Environ. 177, 275–282. https://doi.org/10.1016/j.atmosenv.2017.12.031.

Zheng, J., Shi, X., Ma, Y., Ren, X., Jabbour, H., Diao, Y., Wang, W., Ge, Y., Zhang, Y., Zhu, W., 2020. Contribution of nitrous acid to the atmospheric oxidation capacity in an industrial zone in the Yangtze River Delta region of China. Atmos. Chem. Phys. 20 (9), 5457–5475. https://doi.org/10.5194/acp-20-5457-2020.

Zwozdziak, A., Sówka, I., Willak-Janc, E., Zwozdziak, J., Kwiecińska, K., Balińska-Miśkiewicz, W., 2016. Influence of PM1 and PM2.5 on lung function parameters in healthy schoolchildren—a panel study. Environ. Sci. Pollut. Control Ser. 23 (23), 23892–23901. https://doi.org/10.1007/s11356-016-7605-1.